NANO · MICRO small
www.small-journal.com

Targeted Intracellular Copper Reservoir Enhances Liver Cancer Immunotherapy

Tianao Xie, Yukai Shan, Win Topatana, Taorui Yang, Ruijing Shen, Shijie Li, Jiadong Chen, Yiyuan Zhu, Ziyi Lu, Yeling Liu, Tianen Chen, Yujie Gao, Yuchao Sun, Xiujun Cai, Sarun Juengpanich,* and Mingyu Chen**

Hepatocellular carcinoma (HCC) is commonly classified as a "cold tumor" due to its low immunogenicity and poor response to conventional immunotherapies. Reprogramming the tumor immune microenvironment (TIME) via cuproptosis presents a promising strategy to enhance immunotherapies. Herein, sono-activatable N,N,N',N'-tetrakis(2-pyridinylmethyl)-1,2-ethanediamine (TPEN)-encapsulated cancer-targeted nanoparticles (STCNs) designed to modulate the TIME and potentiate immunotherapy through endogenous cuproptosis are reported, termed "endogenous cuproptosis immunopromotion". STCNs are rapidly internalized by HCC via folate-mediated endocytosis, and ultrasound irradiation triggers the release of TPEN. TPEN then chelates Cu^{2+} from superoxide dismutase, initiating a Fenton-like reaction induced by glutathione that produces reactive oxygen species (ROS) and Cu^{+}. This cascade induces cuproptosis and immunogenic cell death (ICD), promoting robust cytotoxic T lymphocyte infiltration in HCC. The combination of STCNs with anti-programmed cell death protein 1 (PD1) therapy demonstrates significant anti-tumor efficacy in vivo. Moreover, this strategy exhibits similar effectiveness in other solid tumor models, underscoring its broad therapeutic potential. These findings provide a promising framework for enhancing immunotherapy in cold tumors, paving the way for future cancer treatments.

1. Introduction

Hepatocellular carcinoma (HCC) is the sixth most prevalent cancer and the third leading cause of cancer-related mortality worldwide, with few viable treatment alternatives.[1–4] Although cancer immunotherapy, particularly immune checkpoint inhibitors (ICIs), has been gradually incorporated into clinical guidelines as first-line therapies for advanced-stage HCC over the past two decades, the response rate remains far from optimal.[5,6] HCC is classified as a "cold tumor" due to its immune-desert phenotype, which is characterized by the lack of tumor-infiltrating lymphocytes (TILs) in the tumor immune microenvironment (TIME).[7] This immune landscape results in reduced responsiveness to ICIs than a "hot tumor".[6,8] Consequently, strategies aimed at reprogramming the TIME to convert "cold tumors" to "hot tumors" may augment immunologic activity and improve the efficacy of immunotherapy in HCC.

Cuproptosis, a unique form of cell death triggered by excessive copper binding to lipoacylated proteins in the tricarboxylic acid cycle, induces proteotoxic stress responses that culminate in cell death, thereby reprogramming the TIME of various cancers via immunogenic cell death (ICD).[9–12] Dead tumor cells are generally non-immunogenic under normal circumstances but will secrete damage-associated molecular patterns (DAMPs), including

T. Xie, Y. Shan, W. Topatana, R. Shen, S. Li, Z. Lu, T. Chen, Y. Sun, X. Cai, S. Juengpanich, M. Chen
Department of General Surgery
Sir Run-Run Shaw Hospital
Zhejiang University
Hangzhou 310016, P. R. China
E-mail: srrsh_cxj@zju.edu.cn; 21718716@zju.edu.cn; mychen@zju.edu.cn

The ORCID identification number(s) for the author(s) of this article can be found under https://doi.org/10.1002/smll.202502783

DOI: 10.1002/smll.202502783

T. Xie, Y. Shan, W. Topatana, R. Shen, S. Li, Z. Lu, T. Chen, Y. Sun, X. Cai, S. Juengpanich, M. Chen
National Engineering Research Center of Innovation and Application of Minimally Invasive Instruments
Sir Run-Run Shaw Hospital
Zhejiang University
Hangzhou 310016, P. R. China

T. Xie, Y. Shan, W. Topatana, R. Shen, S. Li, Z. Lu, T. Chen, Y. Sun, X. Cai, S. Juengpanich, M. Chen
School of Medicine
Zhejiang University
Hangzhou 310058, P. R. China

M. Chen
State Key Laboratory of Advanced Drug Delivery and Release Systems
Shandong Luye Pharmaceutical Co., Ltd.
Yantai, Shandong 264003, P. R. China

calreticulin (CRT), high mobility group protein B1 (HMGB1), and ATP. These molecules stimulate dendritic cell (DC) maturation to recruit cytotoxic T lymphocytes (CTLs) into the TIME, ultimately enhancing the anti-tumor immune response.[13–15] Additionally, the intracellular reactive oxygen species (ROS) generated by ICD inducers such as cuproptosis play a vital role in amplifying these effects. Despite its promise, the clinical application of cuproptosis-inducing copper ionophores is hindered by challenges such as poor selectivity, limited tumor retention, and a high risk of adverse events.[10,11,16] This highlights the need for alternative strategies to induce cuproptosis without relying on copper ionophores.

To address these challenges, we developed sono-activatable (TPEN)-encapsulated cancer-targeted nanoparticles (STCNs) to induce endogenous cuproptosis and enhance immunotherapy in HCC. STCNs can specifically target HCC cells via folate receptor (FR)-mediated endocytosis and release TPEN upon ultrasound (US) activation. TPEN, a copper chelator, removes Cu^{2+} from superoxide dismutase (SOD), thereby increasing intracellular Cu^{2+} levels. This process, known as the Fenton-like reaction, further generates ROS and increases Cu^{+} levels.[16,17] This leads to oxidative stress that disrupts cellular defenses and induces endogenous cuproptosis. Additionally, the ROS produced activates ICD, stimulating dendritic cell maturation and T-cell infiltration, effectively transforming the immunosuppressive TIME of "cold" HCC tumors into an immunogenic "hot" tumor state. Overall, we proposed an innovative endogenous cuproptosis immunopromotion strategy using STCNs to trigger spatiotemporally controlled endogenous cuproptosis, overcoming the limitations of copper ionophores and significantly enhancing immunotherapy efficacy in HCC (**Figure 1**).

2. Results

2.1. Synthesis and Characterization of STCNs

The synthesis of TPEN-encapsulated NT (NU-1000 introduced the 4,4′,4″,4‴-(Porphine-5,10,15,20-tetrayl) tetrakis(benzoic acid (TCPP) ligand (abbreviated as NT)) (TPEN@NT) was modified from previous work.[18–20] NU-1000 was synthesized as a base metal-organic framework (MOF) and functionalized with porphyrin-based TCPP ligands through ligand exchange to form NT for SDT (Figure S1, Supporting Information), followed by encapsulation of TPEN within the structure. As shown in TEM (**Figure 2a**; Figure S2, Supporting Information), NU-1000, NT, and TPEN@NT maintained a spindle shape with uniform size. Zeta potential and hydrodynamic size measurements confirmed the stepwise assembly of TPEN@NT, with a transition from positive (+38.36 mV) to negative charge (−31.64 mV) and an increase in size from ≈125 to ≈175 nm (Figure 2c,d; Figure S3, Supporting Information). Compared to NU-1000, a new peak at 1700 cm^{-1} corresponding to the C—N bond appeared, resembling the FTIR spectra of TCPP, thereby validating the successful conjugation of NT (Figure S4, Supporting Information).[19] The —C—N═ stretching vibration at 1412 cm^{-1} and the —C—H stretching vibration at 2860 cm^{-1} indicated the successful encapsulation of TPEN, confirming the successful synthesis of TPEN@NT nanoparticles (Figure 2e). ^{1}H NMR analysis further revealed that NT exhibited new peaks between 8.5 and 8.9 ppm, indicating that ≈20% of the H_4TBAPy was effectively substituted by TCPP (Figure S5, Supporting Information).[19] In addition, XRD analysis revealed the crystalline structure of TPEN@NT (Figure 2f). The XRD patterns of NU-1000 and NT are consistent with previously reported studies,[18,19] and TPEN@NT exhibited the same diffraction peaks, indicating that there was no obvious structural change of TPEN@NT during the synthesis process.

Subsequently, sono-responsive cancer-targeted polymeric ligands (SCPLs) were prepared to coat the surface of TPEN@NT, thereby enhancing the biocompatibility and tumor-targeting ability of the obtained STCNs. SCPLs are a block copolymer composed of a hydrophobic chain, a hydrophilic chain, and a singlet oxygen ($^{1}O_2$)-cleavable thioketal (TK) group (Figure S6, Supporting Information). Initially, OCT-PBLA-NH_2 was synthesized through the ring-opening polymerization of β-Benzyl-L-aspartate N-carboxy anhydride (BLA-NCA) using octadecylamine (OCT) as an initiator.[21,22] Next, OCT-PBLA-NH_2 was conjugated with the TK group via acylation to produce COOH-TK-PBLA-OCT, introducing $^{1}O_2$ sensitivity. PEGylated folic acid (FA) (FA-PEG-NH_2) was subsequently attached as the hydrophilic chain, enhancing tumor-targeting specificity and self-assembly ability. The successful conjugation of SCPLs was confirmed via ^{1}H NMR (Figures S7–S10, Supporting Information). Finally, STCNs were synthesized through self-assembly and further explored for structural and functional characterization.

As shown in TEM images (Figure 2a; Figure S11, Supporting Information), STCNs exhibited a clustering distribution due to SCPL coating, which reverted to a discrete distribution upon ultrasound (US) irradiation, demonstrating their sonosensitivity. Zeta potential and DLS revealed that STCNs are negatively charged (−36.42 mV) with an average hydrodynamic size (≈200 nm) (Figure 2c,d), indicating their superior biocompatibility. High-angle annular dark-field scanning transmission electron microscopy (HAADF-STEM) and energy dispersive spectrometry (EDS) demonstrated the uniform distribution of Zr, C, O, N, and S in STCNs (Figure 2b). The X-ray photoelectron spectroscopy (XPS) further validated this chemical state (Figure S12, Supporting Information). Moreover, the —C—O— stretching vibration at 1171 cm^{-1} in FTIR spectroscopy of STCNs is attributed to the PEG chain in SCPLs

T. Yang
College of Pharmaceutical Sciences
Zhejiang University
Hangzhou 310058, P. R. China
J. Chen
Department of Chemistry
Zhejiang University
Hangzhou 310016, P. R. China
Y. Zhu
School of Materials Science and Engineering
Zhejiang University
Hangzhou 310058, P. R. China
Y. Liu
Department of Rheumatology and Clinical Immunology
Peking Union Medical College Hospital
Beijing 100730, P. R. China
Y. Gao
Rizhao Emergency Management Support Center
Rizhao 276800, P. R. China

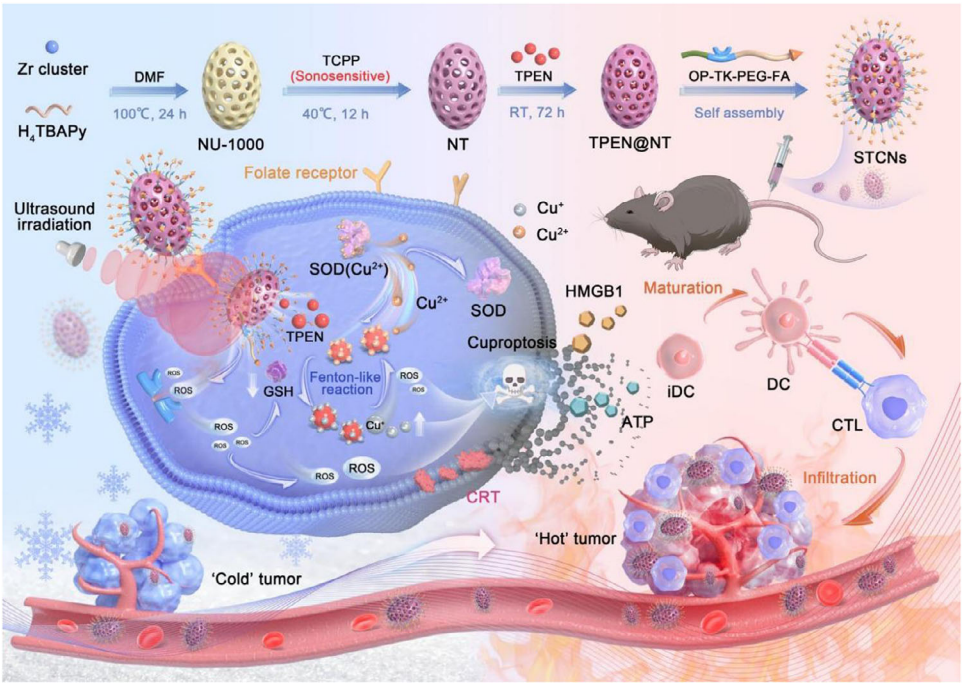

Figure 1. Design and mechanism of STCNs. Schematic illustration of STCNs synthesis and its therapeutic mechanism. STCNs enter and accumulate in the cell via folate-mediated endocytosis. The ultrasound leads to the destabilization of nanoparticle structure, resulting in SDT and the release of TPEN to induce "endogenous" cuproptosis and generate ROS. Finally, dying tumor cells secrete and release DAMPs, such as CRT, ATP, and HMGB1, promoting the infiltration of CTLs into TIME to change it from "cold" to "hot".

(Figure 2e), and the UV–vis absorption spectra of STCNs demonstrate a similar framework structure as NT (Figure S13, Supporting Information). These findings conclusively confirm the successful polymer coating on TPEN@NT, hence the successful synthesis of STCNs. In addition, the same XRD patterns revealed the crystalline structure stability of STCNs, which was consistent with the TEM image (Figure 2f). The synthesis of sono-activatable cancer-targeted nanoparticles (SCNs), sono-activatable TPEN-encapsulated nanoparticles (STNs), and TPEN-encapsulated cancer-targeted nanoparticles (TCNs) was prepared using with similar procedure, but without the addition of TPEN, folic acid conjugation, or TK linker conjugation, respectively.

Next, the stability test revealed no significant changes in particle size or zeta potential after four weeks in PBS, DMEM, and FBS, demonstrating the remarkable physiological stability of STCNs (Figure 2g; Figures S14 and S15, Supporting Information). Subsequently, as shown in the fluorescence spectra, the fluorescence peak of TCPP at 655 nm was similarly observed for STCNs and TCNs with/without US irradiation, indicating the SCPLs modification had almost no effect on the optical properties of the nanoparticles (Figure 2h; Figure S16, Supporting Information). The drug release and sonodynamic activity were further investigated to examine the potential biomedical applications of STCNs. Under physiological conditions, STCNs exhibited minimal TPEN release (≈17%) over 48 h. However, US irradiation triggered a substantial increase, with 89% of TPEN released within 72 h (Figure 2i). This enhanced release was attributed to the $^1O_2$-mediated degradation of the TK group in SCPLs and cavitation effects induced by US activation. In addition, HPLC results revealed that the TPEN drug-loading efficiency of STCNs was ≈8.57% (Figure S17, Supporting Information). Furthermore, we evaluated the sono-responsive ROS generation capacity of STCNs and TCNs using DPBF as the $^1O_2$ indicator. Both STCNs and TCNs demonstrated excellent ROS generation under US irradiation (Figure 2j; Figures S18 and S19, Supporting Information), though ROS levels were slightly lower in STCNs due to partial consumption of $^1O_2$ by the TK group (Figure 2k).[15] These results confirm the successful synthesis and functionality of STCNs, highlighting their potential as a novel platform for precise, sono-responsive cancer treatment.

2.2. Cellular Uptake and Cytotoxicity of STCNs

Previous studies indicate that liver malignancy selectively upregulates FR,[23,24] which serves as a tumor target for STCNs. As demonstrated by fluorescence imaging, STCNs were taken up by human HCC cell line HuH-7 and mouse HCC cell line Hep1-6 and were concentrated primarily in the cytoplasm in a time-dependent manner that peaked at 24 h (**Figure 3a**). Similarly, by TEM observation, we found that tumor cells endocytosed STCNs and allowed them to gradually accumulate in the cytoplasm with exposure duration to STCNs (Figure 3b). Moreover, the same concentration of STCNs was introduced to the mouse hepatocyte cell line AML-12, which resulted in a significantly lower accumulation in the cytoplasm at 24 h compared to HuH-7 and Hep1-6 (Figure S20, Supporting Information). This difference is attributed to the absence of FR in AML-12 cells, suggesting that STCNs can accumulate in the cytoplasm through FR-mediated endocytosis, enabling subsequent tumor-killing

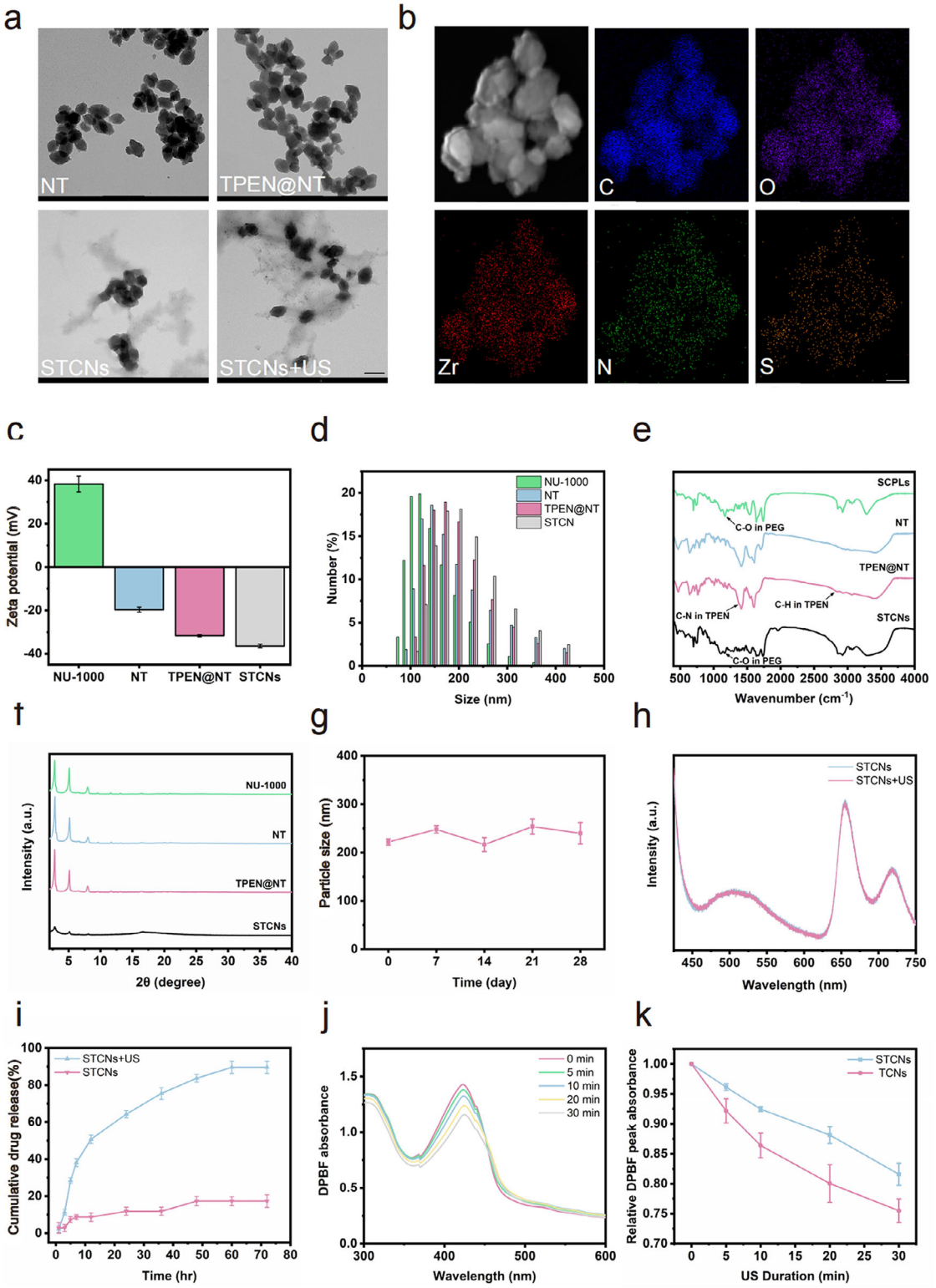

Figure 2. Characterization of STCNs. a) TEM image of NT, TPEN@NT, and STCNs with/without US (scale bar = 200 nm). b) STCNs imaging and EDS mapping (scale bar = 100 nm). c) Zeta potential and d) particle size distribution of NT, TPEN@NT, and STCNs. e) Fourier transform infrared (FTIR) analysis of SCPLs, NT, TPEN@NT, and STCNs. f) X-ray diffraction spectrum of NU-1000, NT, TPEN@NT, and STCNs. g) Stability test of STCNs in PBS. Particle size distribution of STCNs at designated time intervals (0, 7, 14, 21, 28 day). h) TCPP fluorescence intensity from STCNs with/without US irradiation (λex = 405 nm, λem = 655 nm). i) In vitro drug release profile of STCNs. j) DPBF absorbance spectrum changes of STCNs under US irradiation. k) Relative DPBF peak absorbance of STCNs/TCNs under US irradiation. The data are represented as mean ± SD (n = 3).

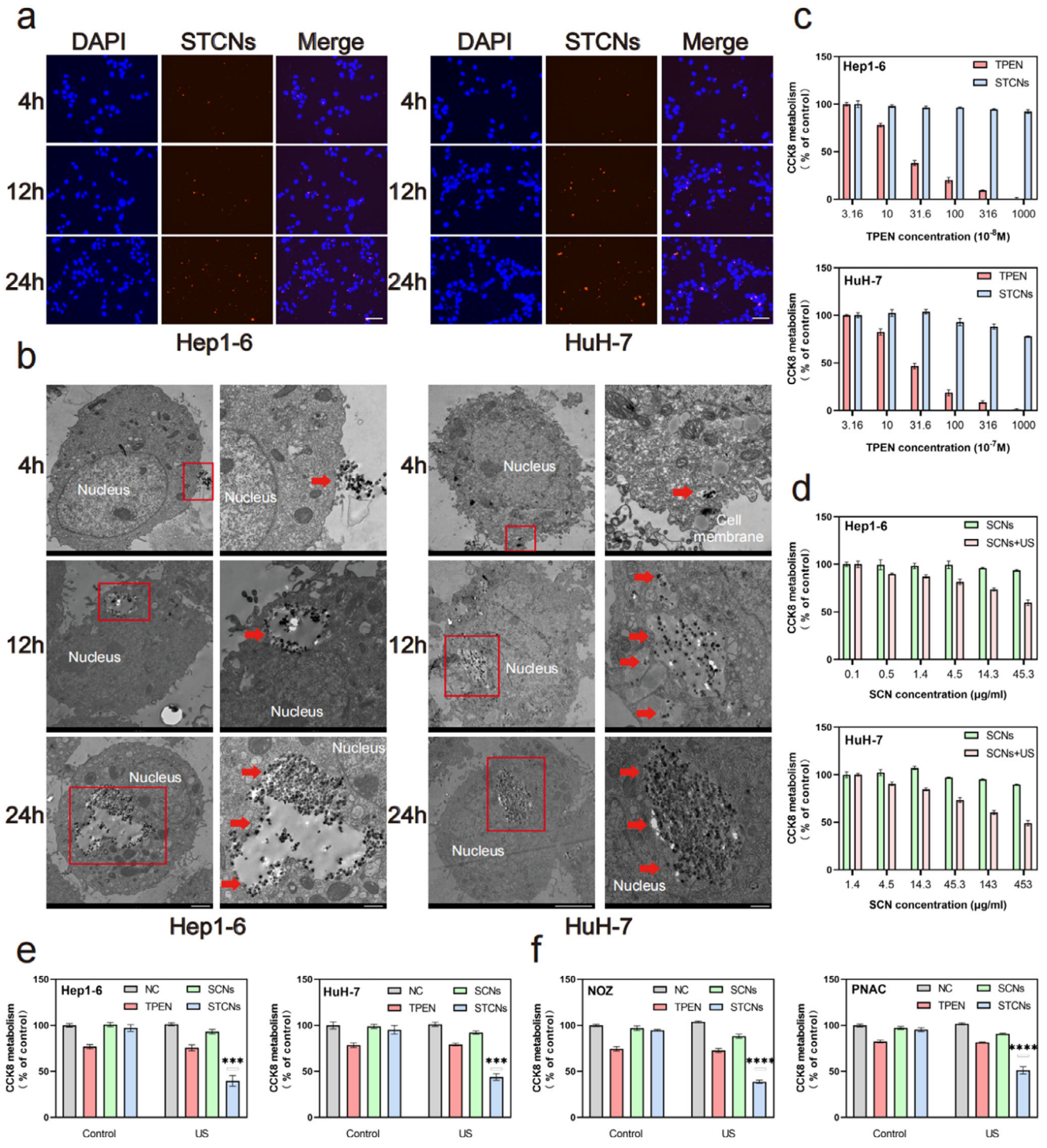

Figure 3. STCNs interactions with HCC cells and antitumor activity. a) Fluorescence images of STCNs cellular uptake by Hep1-6 or HuH-7 cells at different time points. DAPI-stained cells were depicted in blue; STCNs fluorescence signals were depicted in red (scale bar = 100 μm). b) Cryo-TEM images of STCNs cellular uptake by Hep1-6 or HuH-7 cells at different time points (Red arrows indicate STCNs). c) 48 h CCK-8 assays of Hep1-6 or HuH-7 cells treated with different concentrations of TPEN (equivalent to dosage in STCNs) or STCNs. d) 48 h CCK-8 assays of Hep1-6 or HuH-7 cells exposed to different concentrations of SCNs or SCNs with US irradiation for 5 min (1 MHz, 50% duty cycle, 1.0 W·cm^{-2}). e) 48 h CCK-8 assays of Hep1-6 or HuH-7 cells exposed to normal media, TPEN, SCNs, or STCNs with/without US irradiation for 5 min (1 MHz, 50% duty cycle, 1.0 W·cm^{-2}). f) 48 h CCK-8 assays of NOZ or PNAC cells exposed to normal media, TPEN, SCNs, or STCNs with/without US irradiation for 5 min (1 MHz, 50% duty cycle, 1.0 W·cm^{-2}). The data are represented as mean ± SD ($n = 3$). $^{***}p < 0.001$, $^{****}p < 0.0001$.

mechanisms. Next, the cytotoxicity of STCNs and SCNs with US irradiation was tested. No significant cytotoxicity had been shown in STCNs without US irradiation compared with equal concentrations of TPEN monotherapy in both HCC cell lines and normal liver cell line AML-12 (Figure 3c; Figure S21, Supporting Information). Subsequently, the cytotoxicity induced by different concentrations of SCNs (equal to the concentration of STCNs in Figure 3c) with or without US was examined (Figure 3d).

Proliferation detection of HCC cell lines (HuH-7 and Hep1-6) exposed to STCNs was performed to further investigate the cytotoxicity of STCNs. The half maximal inhibitory concentration (IC50) of STCNs + US on Hep1-6 cells was 40.04 nM (based on TPEN dose), which was 4.0 fold lower than that of TPEN administration alone (159.2 μM) (Figure S22a, Supporting Information). Similar effects were observed in HuH-7 cells. The concentration of TPEN below IC50 (1 μM for HuH-7 and 0.1 μM for Hep1-6) was selected for subsequent validation of the antitumor effects of STCNs (Figure S22b, Supporting Information). Notably, the STCNs group showed significantly increased antitumor effects under US irradiation, while the drug-free SCNs did not show a significant proliferation inhibition after US irradiation, indicating an enhanced interaction between TPEN and SDT (Figure 3e). Moreover, due to the excellent in vitro anti-tumor activity of STCNs + US, we further administered it to other solid tumors, including gallbladder carcinoma (GBC-SD and NOZ) cells, colorectal adenocarcinoma (MC38) cells, lung cancer cells (LLC), melanoma (B16F10) cells, and pancreatic cancer cells (PANC-1). Similarly, compared with TPEN monotherapy, a significant cytotoxic effect on different tumors had been observed on STCNs + US treatment, suggesting its high potential for clinical application (Figure 3f; Figure S23, Supporting Information).

2.3. Endogenous Cuproptosis Mechanism and ICD Effect of STCNs

Theoretically, STCNs have a robust anti-tumor ability due to the endogenous cuproptosis effect and subsequent induction of the ICD effect. Initially, TPEN released by the STCNs binds to the Cu^{2+} in SOD, thereby inactivating SOD and blocking the main antioxidant system in the cell. Meanwhile, the binding of Cu^{2+} to TPEN leads to a Fenton-like reaction with GSH, resulting in its reduction to monovalent copper Cu^{+}, which depletes the intracellular antioxidant system through a sustained cycle. Upon reaching a specific stage, due to its higher binding ability with lipoylated proteins, monovalent copper Cu^{+} eventually binds with lipoylated DLAT, forming an insoluble dimer of DLAT that blocks the mitochondrial cycle, induces an endogenous copper death reaction, and ultimately facilitates cell death. Simultaneously, ROS generated by STCNs under US irradiation in the cytoplasm could reduce the GSH levels, promoting cuproptosis. Furthermore, cuproptosis of tumor cells and SDT treatment can induce effective ICD and activate antitumor immunity. Therefore, a certain concentration of TPEN combined with ROS could induce a potent cuproptosis effect on tumors and induce ICD (**Figure 4a**). The combination effects of STCNs were further tested and verified in HCC cell lines, HuH-7 and Hep1-6. As shown in Figure 4b–d and Figure S24 (Supporting Information), the SOD activity, Cu level, and GSH level were measured after different treatments. The ability of TPEN to capture Cu^{2+} from SOD significantly reduced the SOD activity, and an equivalent efficacy to reduce SOD activity in the TPEN and STCNs + US-treated groups can be seen. Compared with the control group, the similar increase of Cu concentration level in TPEN ± US and STCNs + US groups further indicates the ability of TPEN to capture Cu^{2+} from SOD. Additionally, the GSH level significantly decreased in the STCN+US group, reducing to 50%–60%, thereby illustrating the synergistic ability of TPEN (70%) and SDT (80%) to disrupt the antioxidant system in tumor cells. Consequently, the evident oxidation and cuproptosis effects of TPEN and US irradiation were exclusively found in the STCNs group. As depicted in Figure 4e and Figure S25 (Supporting Information), the STCNs + US group decreased Fe-S cluster proteins ferredoxin (FDX1) expression, reducing protein lipoylation of DLAT, which impairs mitochondrial function. Moreover, the increased oligomerization of Cu^{+}-bound lipoylated DLAT aggravated cytotoxicity. The highest oligomerization of lipoylated DLAT was observed in STCNs + US treatment, suggesting its promising cuproptosis effects. In addition, the TPEN ± US and SCNs + US groups generated ≈3-4 and 1.5 fold ROS related to the control group, respectively (Figure 4f,g; Figures S26 and S27, Supporting Information), which reduced the FDX1 expression and DLAT lipoylation level. Moreover, Bio-TEM images demonstrated significant morphological alterations in the mitochondria of the STCNs + US group compared to the control group, including swelling, vacuolization, cristae degradation, and abnormal accumulations (Figure S28, Supporting Information).

In order to better understand the therapeutic mechanism of STCNs on HCC cells, RNA sequencing was performed to identify the different expressions of mRNA in Hep1-6 with or without STCNs treatment. After unsupervised hierarchical clustering, the clear grouping of data within the monotreatment group indicated the reliability of the RNA sequencing data. 2402 differentially expressed genes (DEGs) had been identified within STCNs + US and their counterparts. Of these, 1095 (45.59%) DEGs were downregulated and 1307 (54.41%) DEGs were identified to be upregulated (Figure S29a,b, Supporting Information). Next, Gene Set Enrichment Analysis (GSEA) showed that the DEGs are predominantly associated with immune-related pathways. These findings suggest that treatment with STCNs may stimulate the immune response within the body. (Figure S29c,d, Supporting Information).

Emerging research indicates that both cuproptosis and sonodynamic therapy (SDT) can elicit ICD from dying tumor cells, augmenting anti-tumor immunity.[11,15] Therefore, we considered whether the activation of immune processes induced by STCNs treatment was associated with ICD effects. ICD triggers an immune activation by secreting damage-associated molecular patterns (DAMPs) and promoting the presentation of antigens to dying cells. To further explore this effect, we used confocal microscopy and ATP concentration detection kits to determine the typical changes in ICD-associated DAMPs expression, including increased membrane calmodulin (CRT) exposure, release of high-mobility group box 1 (HMGB1), and intracellular adenosine triphosphate (ATP) efflux. The most apparent CRT aggregation and HMGB1 downregulation were observed in the STCNs + US group (Figure 4h; Figures S30 and S31, Supporting Information).

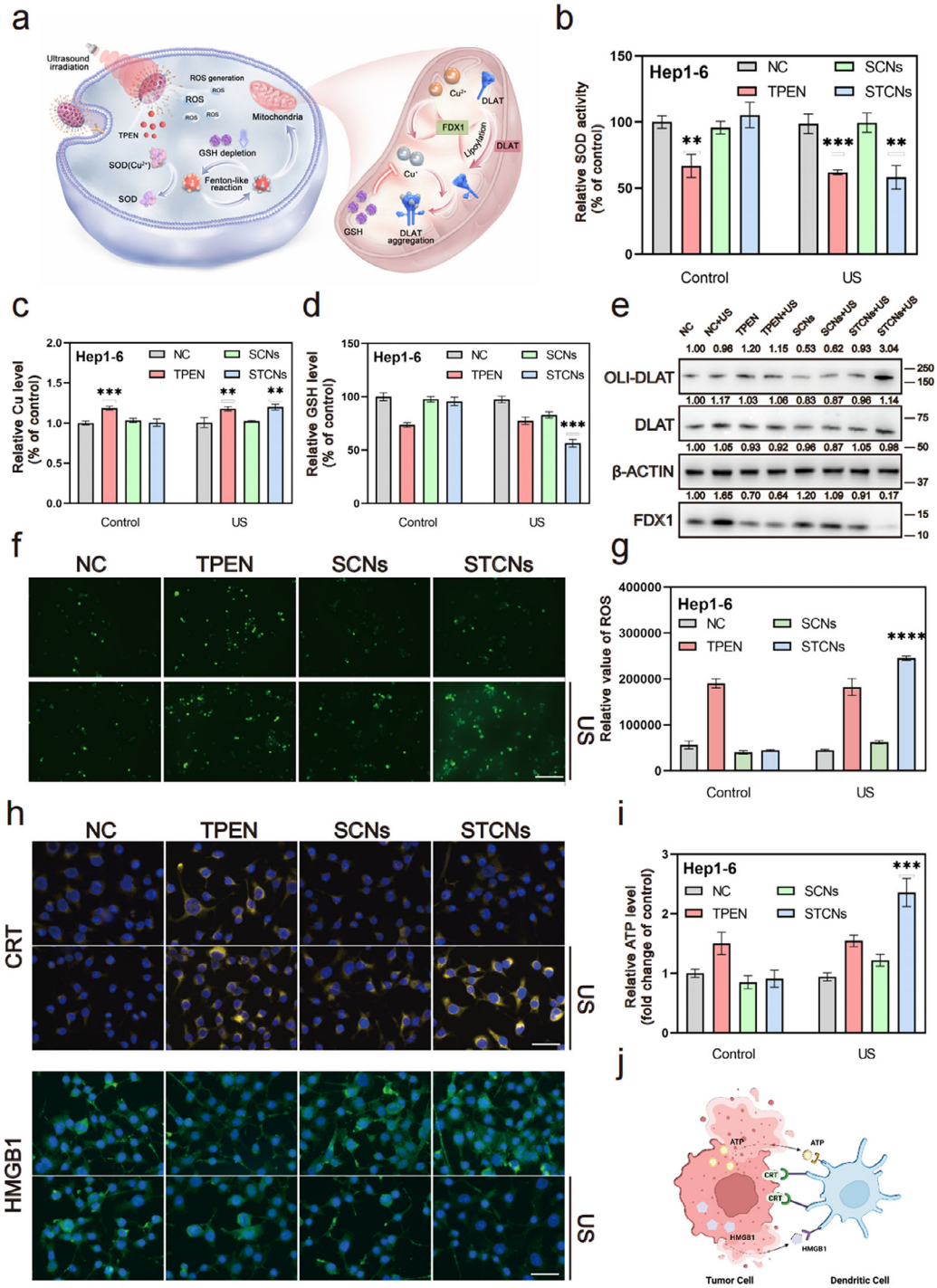

Figure 4. Evaluation of SDT-amplified endogenous cuproptosis and ICD induction of STCNs. a) Schematic illustration of STCNs underlying endogenous cuproptosis mechanism. b) Activity of SOD in Hep1-6 cells exposed to normal media, TPEN, SCNs, or STCNs with/without US irradiation for 5 min (1 MHz, 50% duty cycle, 1.0 W·cm^{-2}). c) Relative level of Cu in Hep1-6 cells exposed to normal media, TPEN, SCNs, or STCNs with/without US irradiation for 5 min (1 MHz, 50% duty cycle, 1.0 W·cm^{-2}). d) Relative level of GSH in Hep1-6 cells exposed to normal media, TPEN, SCNs, or STCNs with/without US irradiation for 5 min (1 MHz, 50% duty cycle, 1.0 W·cm^{-2}). e) Western blot for OLI-DLAT, DLAT, β-Actin, and FDX1 of Hep1-6 cells exposed to normal media, TPEN, SCNs, or STCNs with/without US irradiation for 5 min (1 MHz, 50% duty cycle, 1.0 W·cm^{-2}). f) Intracellular ROS observation and g relative value of ROS of Hep1-6 cells treated as indicated (scale bar = 275 μm). h) CRT and HMGB1 immunofluorescence images of Hep1-6 cells exposed to normal media, TPEN, SCNs, or STCNs with/without US irradiation for 5 min (1 MHz, 50% duty cycle, 1.0 W·cm^{-2}) (CRT/HMGB1 fluorescence signals are depicted in yellow/green and DAPI-stained cells are depicted in blue) (scale bar = 50 μm). i) Extracellular ATP level measurements in Hep1-6 cells exposed to normal media, TPEN, SCNs, or STCNs with/without US irradiation for 5 min (1 MHz, 50% duty cycle, 1.0 W·cm^{-2}). j) Schematic diagram of ICD-triggered DC maturation. The data are represented as mean ± SD ($n = 3$). $^{**}p < 0.01$, $^{***}p < 0.001$, $^{****}p < 0.0001$.

Furthermore, the ATP secretion levels were significantly increased after STCNs + US treatment (Figure 4i; Figure S32, Supporting Information). Additionally, the expressions of CD86 and CD80 expressions in mouse bone marrow-derived dendritic cells (BMDCs) were significantly increased after STCNs + US treatment (Figures S33 and S34, Supporting Information), indicating that STCNs can effectually facilitate DCs maturation with US irradiation, which may further activate the immune system and effectively eliminate tumors. These results revealed that STCNs-mediated cuprotosis and SDT effectively triggered ICD, subverting the immunosuppressive effects of tumors by enhancing APCs activation (Figure 4j).

2.4. Therapeutic Efficacy Evaluation and Immune Response Activation of STCNs

To further verify the anti-tumor ability of US-activated STCNs in subcutaneous HCC-bearing mice models, we randomly divided the mice into 8 groups, including PBS, TPEN (1.5 mg kg^{-1}), SCNs (16 mg kg^{-1}), STCNs (17.5 mg kg^{-1}, equal dose of TPEN) under 15 min US irradiation or not at 8 h after injection (1 MHz, 50% duty cycle, 1.0 W cm^{-2}), and administered via tail vein injection three times a week to record the tumor growth curve (**Figure 5a**). As depicted in Figure 5b,c, tumor growth was significantly inhibited in mice in the STCNs + US group and showed minimal volume compared with other groups, indicating its efficient anti-tumor effect. Moreover, mice treated with TPEN or SCNs + US exhibited a moderately reduced tumor burden, while mice treated with SCNs and STCNs did not show any significant tumor reduction. In addition, the results in the PBS + US and TPEN + US treatment groups indicated that US irradiation alone did not reduce tumor burden.

A normal trend of weight gain could be observed in tumor-bearing mice treated with STCNs + US, implying its negligible adverse effects (Figure S35, Supporting Information). In contrast, significant weight loss was observed in the PBS group, PBS + US group, SCNs group, or STCNs-treated group, which was mainly caused by increased tumor burden. Of note, the median survival time of STCNs + US-treated mice (74 days) was significantly longer than that of PBS-treated mice (38 days), while TPEN (49 days), TPEN + US (51 days), and SCNs + US (45 days) treated mice showed moderate prolongation (Figure 5d). Hematoxylin and eosin (H&E) staining showed that the anti-tumor effect of each group was consistent with the tumor growth. In addition, histological analysis showed that STCNs + US treatment greatly reduced the tumor cell proliferation index (Ki-67), which verified the potent anti-tumor effect of STCNs in vivo (Figure S36, Supporting Information).

To evaluate the activation of the ICD effect, flow cytometry was used to analyze the distinct populations of various immune cells (Figures S37 and S38, Supporting Information). The contents of dendritic cells (DCs ($CD80^+CD86^+$)) in tumor-draining lymph nodes for the control (2.6 ± 0.1%), SCNs (2.6 ± 0.3%), and STCNs group (2.5 ± 0.1%) were similar to 2.8% ± 0.2% for the control + US groups (Figure S39, Supporting Information). This suggests that the US alone does not affect the anti-tumor immune system. In the TPEN ± US group and SCNs + US group, the DCs content was 3.2% ± 0.1%, 3.3% ± 0.1%, and 3.5% ± 0.2%, respectively, which was higher than the control (1.3 fold) group. The highest DCs number was observed in the STCNs + US group (6.1 ± 0.2%), which was 2.4 fold higher related to the control and STCNs without US groups. The contents of marrow-derived suppressor cells (MDSCs, $CD11b^+Gr1^+$) in the tumor were then measured. The lowest proportion of MDSCs was observed for the STCNs + US group (21.4 ± 2.3%), which was 2.3 fold lower than the control and STCN without US groups (Figure S40, Supporting Information). In the TPEN ± US group and SCNs + US group, the MDSCs content was 39.1% ± 2.3%, 40.2% ± 2.7%, and 40.9% ± 1.6%, respectively, which was lower than the PBS (1.2 fold) treatment group. These results indicated the ability of STCNs + US to effectively activate DCs and inhibit MDSCs. Next, effector T cells (CD3+CD8+ T cells and CD3+CD4+ T cells), in HCC tumors after the above-mentioned treatments, were detected. The proportions of those T cells were significantly increased after the administration of TPEN and STCNs + US treatment. In STCNs + US treatment, the infiltration of CD3+CD8+ T cells was the highest (42.4 ± 4.6%), which was a 2.5 fold increase related to PBS (17.1 ± 3.2%) and STCNs without US (16.5 ± 6%) groups (Figure S41, Supporting Information). The highest CD3+CD4+T cell content (30.6 ± 1.5%) was also detected in STCNs + US treatment, a 1.7 fold higher than control (18.1 ± 1.0%) and STCNs without US (18.2 ± 2.9%) groups (Figure S42, Supporting Information). This is potentially due to the immune system activation by the ICD effect, which subsequently activates T cells. Furthermore, the proportion of critical immunosuppressive regulatory T cells (Tregs) in primary tumors was also analyzed. Due to the ICD and SDT effect that could induce a systemic immune response, the treatment of TPEN and SCNs + US decreased the aggregation of Tregs in tumors (Figure S43, Supporting Information). Importantly, the Treg cell content in STCNs + US groups significantly reduced to 1.3 ± 0.5% from the combined effect of ICD and SDT, which reversed the immunosuppressive microenvironment. Immunofluorescence imaging of tumor tissues in different treatment groups further verified the strong immune system activation ability of STCNs + US (Figure 5e). Overall, these results demonstrate that STCNs-mediated SDT and cuproptosis effectively triggered the ICD effect, transforming "cold" HCC tumors into an immunogenic "hot" tumor state.

The immune-enhancing effect provided by STCNs + US-induced SDT and ICD effect offered a conducive environment for improved immune checkpoint inhibitor treatment. Thus, we investigated whether STCNs + US treatment could synergize with the PD-1 blockade to improve the response rates of therapeutic effects on subcutaneous HCC mouse models. Hep1-6 bearing mice received distinct treatments via tail vein injection, including PBS, anti-PD-1 (200 μg), and anti-PD-1 (200 μg) + STCNs (17.5 mg kg^{-1}) + US, and the tumor growth was recorded three times a week for 10 days (Figure 5f). As shown in Figure 5g and Figure S44 (Supporting Information), the anti-PD-1 monotherapy group showed a slowing trend in tumor growth, while tumor volume was decreased dramatically in STCNs + anti-PD-1 + US group, demonstrating the promising combined anti-tumor effect of STCNs with PD-1 under US activation.

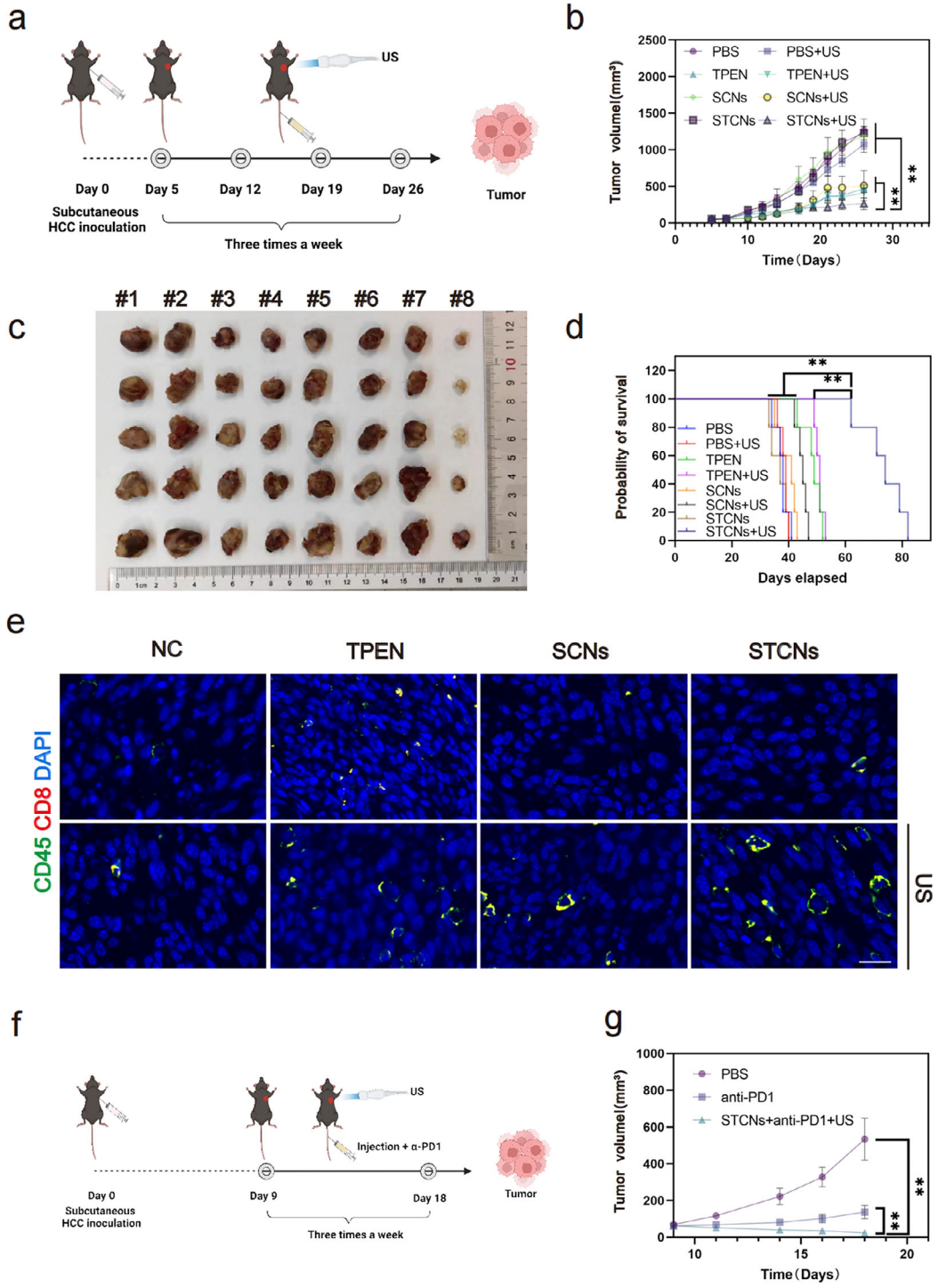

Figure 5. Evaluation of therapeutic efficacy and immune response activation of STCNs. a) Schematic illustration of experimental procedure for therapeutic efficacy evaluation. b) Tumor volume changes in different groups during treatment of subcutaneous HCC model (PBS, PBS + US, TPEN, TPEN + US, SCNs, SCNs + US, STCNs, and STCNs + US) ($n = 5$ biologically independent samples). c) Tumor images after 21 days of treatment in different groups (#1: PBS; #2: PBS + US; #3: TPEN; #4: TPEN + US; #5: SCNs; #6: SCNs + US; #7: STCNs; #8: STCNs + US). d) Survival curves of subcutaneous HCC model of mice in different groups (PBS, PBS + US, TPEN, TPEN + US, SCNs, SCNs + US, STCNs, and STCNs + US) ($n = 5$ biologically independent samples). e) Fluorescent images of $CD45^+$ cells and $CD8^+$ T cell staining in tumor tissues after various treatments (normal media, TPEN, SCNs, or STCNs with/without US irradiation for 5 min (1 MHz, 50% duty cycle, 1.0 W·cm^{-2})). f) Schematic illustration of therapeutic efficacy evaluation through combining STCNs with α-PD1. g) Tumor volume changes in different groups during treatment of subcutaneous HCC model (PBS, α-PD1, and STCNs + α-PD1 + US) ($n = 5$ biologically independent samples). The data are represented as mean ± SD ($n = 3$). $^*p < 0.05$, $^{**}p < 0.01$, $^{***}p < 0.001$, $^{****}p < 0.0001$.

2.5. Tumor-Targeting Ability, Biodistribution, and Biosafety of STCNs

In vivo fluorescence imaging (FL) was performed to verify the tumor-targeting capacity and distribution of STCNs. 4 h after STCNs injection, STCNs were widely distributed throughout the body. At 8 and 12 h after injection, the STCNs group showed stronger FL intensity at the primary tumor location than TCPP and STNs, suggesting robust tumor targeting and retentive ability of STCNs through folate-mediated endocytosis (Figure S45, Supporting Information). STCNs group showed similar accumulation at tumor sites compared with free TCPP at 8 and 12 h post-injection, which was mainly caused by the FR-mediated endocytosis effect. A decrease in whole-body fluorescence had been shown at 36 h after injection, indicating that the nanoparticles were gradually excreted during circulation. To identify the distribution and metabolism of STCNs in the systemic circulation, tumors and corresponding vital organs (kidney, spleen, lung, heart, liver) were removed from C57BL/6J mice at pre-, 1, 4, 8, 12, 24, and 36 h after STCNs injection for ex vivo FL imaging (**Figure 6a**). FL intensity at different time points suggested that the liver, kidney, and tumor were the predominant organs of STCNs distribution. The overall distribution profile of STCNs was similar to the in vivo imaging findings described above. These results indicate that STCNs have a certain circulation period, and the in vivo tumor targetable ability and retention ability are robust, allowing them to efficiently accumulate in tumor tissues. To further assess biosafety, the systemic toxicity of STCNs under US activation was assessed at day 40. Compared with the healthy mice, there were no significant changes in hematological parameters and liver function in STCNs treated mice (Figure 6b,c). It was further confirmed by H&E staining results of major organs (kidney, spleen, lung, heart, and liver) (Figure 6d). In addition, the pharmacokinetic analysis of STCNs revealed a blood circulation half-life of ≈5 h (Figure S46, Supporting Information).

3. Discussion

Immunotherapy has emerged as a cornerstone in the treatment of advanced-stage cancers. However, its efficacy is limited in immune "cold" tumors, such as HCC, which exhibit poor cytotoxic T lymphocyte (CTL) infiltration.[5,25] Recent research indicates that cuproptosis, a copper-dependent form of cell death, can go beyond directly killing tumor cells by triggering ICD through ROS generation. This process can enhance CTL infiltration into TIME and activate robust anti-tumor immune responses.[9–11,26–28] Traditional ionophores, such as disulfiram (DSF) and elesclomol (ES), aim to induce copper overload to trigger cuproptosis. Despite their promise, these approaches face significant challenges, including rapid drug clearance, off-target toxicity, and cancer cells' robust antioxidant defenses, such as superoxide dismutase (SOD) and glutathione (GSH).[29–32] To overcome these limitations, we propose a novel "endogenous cuproptosis immunopromotion" strategy using sono-activatable TPEN-encapsulated cancer-targeted nanoparticles (STCNs). TPEN selectively extracts Cu^{2+} from SOD, disrupting the cellular copper reservoir and increasing free intracellular copper levels. This promotes a Fenton-like reaction, where Cu^{2+} is reduced to Cu^{+} by intracellular GSH, catalyzing the decomposition of hydrogen peroxide into highly cytotoxic hydroxyl radicals (•OH).[16,17] This ROS generation culminates in endogenous cuproptosis independent of exogenous copper supplementation and promotes ICD-mediated CTL infiltration into the TIME.

Recent advances in physical therapeutic methods, such as sonodynamic therapy (SDT) and photodynamic therapy (PDT), offer significant advantages over traditional treatments due to their non-invasive, ROS-based mechanisms.[33,34] SDT, in particular, achieves greater tissue penetration of up to 10 cm compared to PDT, making it ideal for treating deep-seated tumors like HCC, gallbladder cancer, and pancreatic cancer.[35–37] However, conventional organic sonosensitizers, such as porphyrins, suffer from poor biological stability and high toxicity, limiting their clinical use.[37–39] STCNs overcome these challenges by integrating TPEN with SDT for a synergistic anti-tumor effect. The deep tissue penetration of US activates STCNs in situ, triggering ROS generation and amplifying endogenous cuproptosis by disrupting antioxidant defenses. Copper, a key cofactor for enzymes like metallothionein (MT) and SOD, forms an internal copper reservoir in cancer cells[16,40,41] which leaks to generate ROS, inducing cuproptosis independent of exogenous copper. This strategy not only disrupts cancer cell defenses but also significantly enhances CTL infiltration into the TIME, reprogramming the environment for improved immunotherapy outcomes. Additionally, STCNs feature a folate-modified surface for selective targeting of HCC cells with high FR expression, minimizing off-target effects and systemic toxicity. The incorporation of modular MOFs and a sono-responsive coating further improves drug stability and delivery precision.[42–44] Under physiological conditions, TPEN release is minimal (≈17%), but US activation triggers a significant increase (≈89%) in TPEN release, driven by $^{1}O_{2}$-induced cleavage and cavitation effects.[15,45] This spatiotemporal control ensures biosafety during circulation while maximizing therapeutic specificity. Furthermore, the use of NT to enhance SDT via US irradiation amplifies cuproptosis and boosts CTL infiltration in the TIME by ≈1.3 times, extending the survival period of tumor-bearing mice.[19,46,47] This synergistic approach not only promotes endogenous cuproptosis but also sensitizes cancer cells to oxidative stress, reprogramming the TIME to enhance immunotherapy outcomes.

The innovative design of STCNs provides unique advantages in treating immune-desert tumors. By combining endogenous cuproptosis with SDT, STCNs overcome the spatial and temporal limitations of traditional exogenous approaches. The targeted delivery and modular flexibility of STCNs allow for tailored therapeutic strategies based on tumor characteristics, enabling personalized cancer treatment. Moreover, STCNs demonstrate superior anti-tumor efficacy in deep-seated tumors due to the enhanced penetration of US, making them applicable for treating challenging cancers such as gallbladder and pancreatic cancers. Most importantly, this study introduces a transformative approach to igniting immune-desert tumors, converting them into immune-active states while improving the outcomes of cancer immunotherapy. By leveraging the synergistic effects of endogenous cuproptosis, ROS generation, and CTL infiltration, STCNs represent a promising strategy to address the limitations of conventional therapies and advance the clinical management of HCC and other immune "cold" tumors.

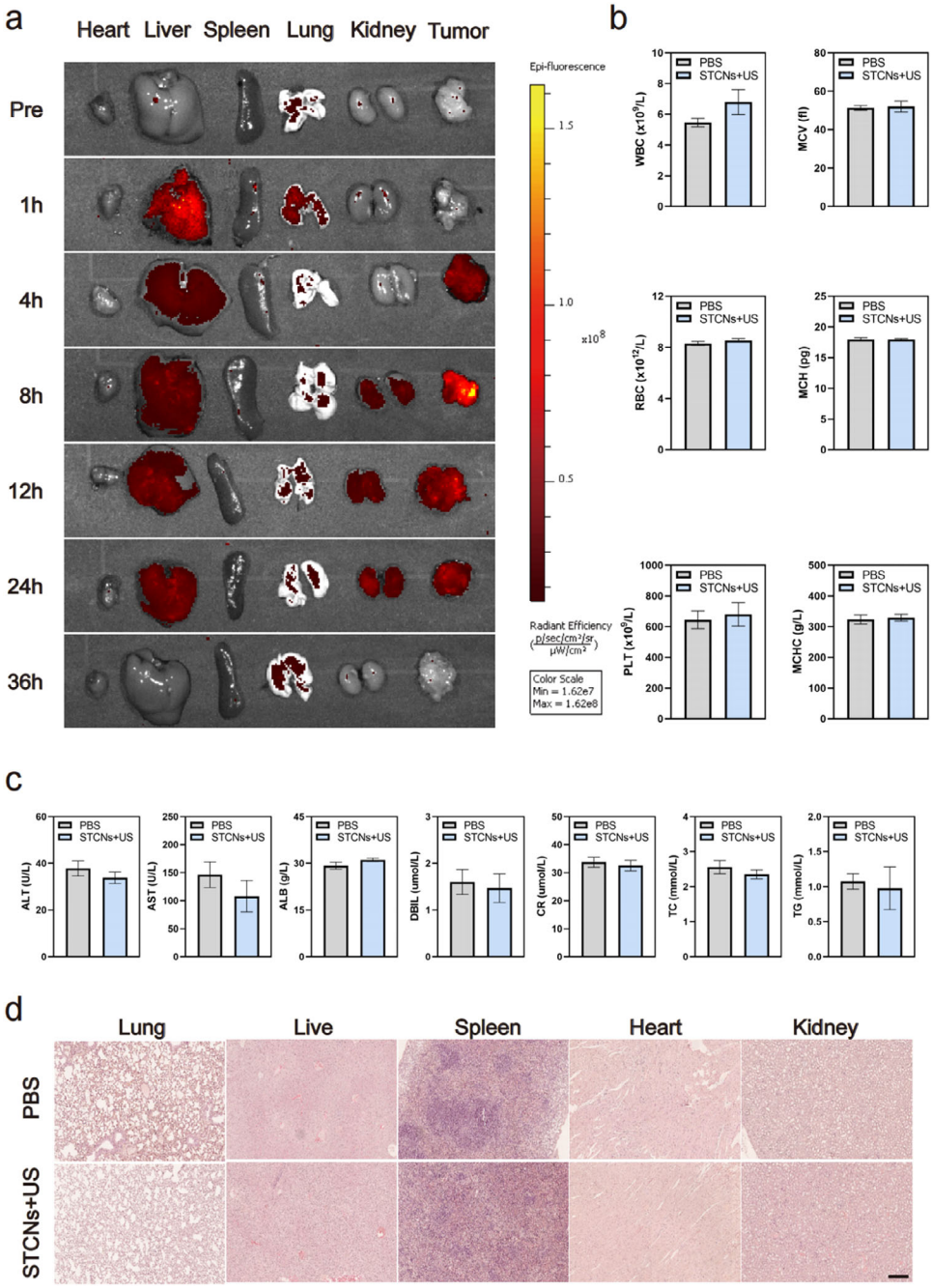

Figure 6. STCNs tumor-targeting ability, biodistribution, and biosafety. a) Ex vivo fluorescence (FL) images of tumors and other organs collected from mice treated with STCNs after intravenous injection at different time points (pre, 1, 4, 8, 12, 24, 36 h). b) Healthy mice were intravenously injected three times a week for a total of 9 times with 200 µL of PBS or STCNs solution (17.5 mg kg^{-1}, irradiated by ultrasound for 15 min at 8 h post-injection, 1 MHz, 50% duty cycle, 1.0 W·cm^{-2}) and sacrificed at day 30 for hematological analysis. c) Healthy mice were intravenously injected three times a week for a total of 9 times with 200 µL of PBS or STCNs solution (17.5 mg kg^{-1}, irradiated by ultrasound for 15 min at 8 h post-injection, 1 MHz, 50% duty cycle, 1.0 W·cm^{-2}) and sacrificed at day 30 for blood biochemical analysis. d) H&E staining analysis for STCNs in vivo toxicology (scale bar = 250 µm). The data are represented as mean ± SD (n = 3 mice per group). ALB: albumin; ALT: alanine aminotransferase; AST: aspartate aminotransferase; CR: creatinine; DBIL: direct bilirubin; MCH: mean corpuscular hemoglobin; MCHC: hemoglobin concentration; MCV: mean corpuscular volume; PLT: platelets; RBC: red blood cells; TC: total cholesterol; TCPP: tetrakis (4-carboxyphenyl) porphyrin; TG: triglyceride; WBC: white blood cells.

4. Conclusion

In conclusion, the unique design of STCNs offers notable advantages for treating immune-desert ("cold") tumors. First, folic acid acts as a tumor-specific targeting ligand, enabling rapid accumulation of STCNs in the cytoplasm of HCC cells via endocytosis, which reduces both the required drug dosage and the risk of off-target effects. Second, the sono-responsive polymer coating significantly improves STCNs biocompatibility, preventing premature exposure of TPEN in circulation and minimizing drug toxicity. Third, STCNs induce "endogenous" cuproptosis in cancer cells, overcoming the spatial and temporal limitations of exogenous cuproptosis, thereby enhancing anti-tumor activity. Fourth, the US provides deep tissue penetration, effectively activating STCNs for SDT in deep tumors while sparing normal tissues from damage. This also disrupts the intracellular antioxidant defense system, synergizing with the cuproptosis effect to promote anti-tumor activity, enhance CTL infiltration in the TIME, and improve immunotherapeutic efficacy. Finally, STCNs can be flexibly modified to tailor treatment to the specific characteristics of different tumors, offering considerable clinical application potential. Most importantly, this study introduces a novel approach to activating "cold" tumors, providing a fresh perspective on immunotherapy.

5. Experimental Section

Ethical Regulations: All animal handling protocols and experiments were approved by the Guidelines for Care and Use of Laboratory Animals of Zhejiang University (Protocol No. 24594). In accordance with the requirements of the Laboratory Animal Welfare and Ethics Committee of Zhejiang University, the size of the subcutaneous tumor and body tumor of mice must not exceed 1000 mm^3, in which the diameter of any dimension must be less than 10 mm. Once this size was reached, euthanasia must be performed. In every animal experiment described in this article, the maximal tumor size/burden of the mouse was never exceeded.

Materials: All precursors and solvents were obtained commercially and used without further purification. β-benzyl-L-aspartate (BLA), bis-(trichloromethyl)-carbonate (triphosgene), tetrahydrofuran (THF), hexane, N,N-dimethylformamide (DMF), dichloromethane (DCM), dimethyl sulfoxide (DMSO), Octadecylamine (OCT), N-(3-dimethylaminopropyl)-N'-ethylcarbodiimide hydrochloride (EDC), N-hydroxysuccinimide (NHS), Folic acid PEG amine (FA-PEG-NH_2), $ZrOCl_2$•$8H_2O$, 4-Biphenylcarboxylic acid (BPCA), 4,4′,4″,4‴-(Porphine-5,10,15,20-tetrayl) tetrakis(benzoic acid) (TCPP), sodium hydroxide (NaOH), 1,3-diphenylisobenzofuran (DPBF), 5,5-dimethyl-1-pyrroline N-oxide (DMPO), acetonitrile (ACN), and trifluoroacetic acid (TFA) were purchased from Aladdin Co. (China). Deionized water and 2,2′-[propane-2,2-diylbis(thio)]diacetic acid (COOH-TK-COOH) were purchased from Macklin Co. (China). Diethyl ether, hydrochloric acid (HCl), acetone, and ethanol were purchased from Sinopharm Co. (China). 4,4′,4″,4‴-(1,9-dihydropyrene-1,3,6,8-tetrayl)tetrabenzoic acid (H_4TBAPy) was purchased from Leyan Co. (China). N,N,N',N'-Tetrakis(2-pyridylmethyl)ethylenediamine (TPEN) was purchased from MCE Co. (USA).

β-Benzyl-L-aspartate N-carboxy anhydride (BLA-NCA) Synthesis: BLA-NCA was prepared according to the previous work.[21,22] Briefly, β-benzyl-L-aspartate (BLA) (10.0 g, 44.8 mmol) and triphosgene (10.0 g, 33.7 mmol) were mixed in anhydrous tetrahydrofuran (THF) (200 mL) and stirred at 60 °C for 3 h under argon gas. Next, the mixture was cooled to room temperature and filtered. The product was purified through precipitation with cool hexane three times, filtered, and dried under vacuum at room temperature.

Octadecylamine-poly(β-benzyl-L-aspartate) (OCT-PBLA) Synthesis: To prepare OCT-PBLA, BLA-NCA (3.0 g, 12.0 mmol) was polymerized in a mixture of N,N-dimethylformamide (DMF) (20 mL) and dichloromethane (DCM) (50 mL) with the primary amino group of octadecylamine (OCT) (0.3 g, 1.2 mmol) at 40 °C for 48 h under argon gas. The reaction mixture was rotovapped at 40 °C for 10 min under vacuum to remove the DCM. Finally, the solution was then precipitated via the slow addition of HCl aqueous solution (0.1 mol L^{-1}, 20 mL) followed by centrifugation, dialyzed against deionized water (MWCO: 1000 Da), and lyophilized to obtain OCT-PBLA.

OCT-PBLA-TK-COOH Synthesis: To prepare OCT-PBLA-TK-COOH, COOH-TK-COOH (250 mg, 1.11 mmol), N-(3-dimethylaminopropyl)-N'-ethylcarbodiimide hydrochloride (EDC) (191.7 mg, 1.0 mmol), and N-hydroxysuccinimide (NHS) (115.09 mg, 1.0 mmol) were dissolved in DCM (20 mL) and stirred for 6 h at room temperature under argon gas. Next, a solution of OCT-PBLA (253 mg, 0.11 mmol) in DCM (5 mL) was added dropwise to the solution and stirred for 48 h at room temperature under argon gas. Finally, the reaction mixture was then purified via precipitation in excess of diethyl ether three times, dialyzed against deionized water (MWCO: 1000 Da), and lyophilized to obtain OCT-PBLA-TK-COOH.

Sono-Responsive Cancer-Targeted Polymeric Ligand (SCPL) Synthesis: To prepare SCPL, OCT-PBLA-TK-COOH (255 mg, 0.1 mmol), N-(3-dimethylaminopropyl)-N'-ethylcarbodiimide hydrochloride (EDC) (19.17 mg, 0.1 mmol), and N-hydroxysuccinimide (NHS) (11.51 mg, 0.1 mmol) were dissolved in DCM (20 mL) and stirred for 6 h at room temperature under argon gas. Next, a solution of FA-PEG-NH_2 (MW: 2000 Da, 200 mg, 0.1 mmol) in DCM (5 mL) was added dropwise to the solution and stirred for 48 h at room temperature under argon gas. Finally, the reaction mixture was then purified via precipitation in excess of diethyl ether three times, dialyzed against deionized water (MWCO: 3500 Da), and lyophilized to obtain FA-PEG-TK-PBLA-OCT (SCPL).

NU-1000 Synthesis: To prepare NU-1000, $ZrOCl_2.8H_2O$ (97 mg, 0.3 mmol) and 4-Biphenylcarboxylic acid (BPCA) (1.6 g, 8.0 mmol) were dissolved in DMF (8 mL) and stirred at 80 °C for 1 h under argon gas. Meanwhile, 4,4′,4″,4‴-(1,9-dihydropyrene-1,3,6,8-tetrayl)tetrabenzoic acid (H_4TBAPy) (55 mg, 0.08 mmol) and NaOH aqueous solution (1 mol L^{-1}, 108 µL) were dissolved in DMF (3 mL). After 1 h, the reaction solution was cooled to room temperature, then the H_4TBAPy solution was added to it and stirred at 100 °C for 24 h under argon gas. Next, the reaction mixture was cooled to room temperature, followed by centrifugation, and washed with DMF 3 times to obtain unactivated NU-1000. The unactivated NU-1000 was dissolved in the mixture of DMF (20 mL) and HCl aqueous solution (8 mol L^{-1}, 4 mL) and stirred at 100 °C for 24 h. After activation, the reaction mixture was cooled to room temperature, followed by centrifugation, and washed with DMF and acetone 3 times. Finally, the NU-1000 was dried under vacuum at 120 °C for 12 h.

NU-1000 Introduced the TCPP Ligand (Abbreviated as NT) Synthesis: To prepare NT, NU-1000 (30 mg) and TCPP (45 mg) were dissolved in DMF (45 mL) and stirred at 40 °C for 12 h. Next, the reaction mixture was cooled to room temperature, followed by centrifugation, and washed with DMF and ethanol 3 times. Finally, the NT was dried under vacuum at 50 °C for 12 h.

TPEN@NT Synthesis: To prepare TPEN@NT, NT (10 mg) and TPEN (1 g) were dissolved in ethanol (5 mL). The reaction mixture was then stirred for 72 h at room temperature, followed by centrifugation, and washed with ethanol once. The resulting TPEN@NT was re-dispersed in DMSO.

STCNs Synthesis: To prepare STCNs, FA-PEG-TK-PBLA-OCT (20 mg, 4 µmol) and TPEN@NT (500 µL, 10 mg mL^{-1}) were dissolved in DMSO (1 mL) and stirred for 30 min at room temperature. Next, the mixture was added dropwise into the deionized water (10 mL) under vigorous stirring and stirred for 3 h at room temperature to induce TPEN@NT encapsulation and micelle formation. The reaction solution was dialyzed against deionized water (MWCO: 7000 Da) for 24 h, followed by centrifugation with a spin filter (Millipore; MWCO: 10 kDa, 10,000 g, 10 min), and washed with deionized water three times to remove excess ligands. Finally, the resulting TPEN@NT-SCPL (STCNs) was re-dispersed in PBS. The synthesis of SCNs, STNs, and TCNs was prepared using with same process, but

without the addition of TPEN, folic acid conjugation, or TK linker conjugation, respectively.

Characterization: Transmission electron microscopy (TEM) was taken with HT-7700 (Hitachi, Japan) at 120 kV for morphology characterization. High-angle annular dark-field scanning transmission electron microscopy (HADFF-STEM) imaging and mapping were conducted on Tecnai G2 F20 S-Twin (FEI, USA). Zeta potentials and dynamic light scattering (DLS) were conducted on Zetasizer Nano ZSU3200 (Malvern Panalytical, UK). ^{1}H NMR analysis was conducted on Ascend 600 (Bruker, Swiss) using DMSO-*d6* as the solvent (NU-1000 and NT need to be dissolved in D_2SO_4 first). FTIR analysis was conducted on Nicolet AVA TAR370 (ThermoFisher, USA). Brunauer–Emmett–Teller (BET) analysis was conducted on AUTOSORB-IQ2-MP (Quantachrome Instruments, USA). Thermogravimetric analysis (TGA) was conducted on TA-Q500 (TA Instruments, USA). Absorption spectrum was conducted on an Agilent Cary 6 (Marshall Scientific, USA). Fluorescence spectrum was conducted on IHR550 (Horiba, USA). Electron spin resonance (ESR) measurements were conducted on an A300 Spectrometer (Bruker, Swiss), using a 1.0 mm quartz capillary. X-ray diffraction (XRD) patterns were conducted on D8 ADVANCE (Bruker, Swiss). X-ray photoelectron spectroscopy (XPS) was conducted on AXIS SUPRA (Krato, UK). High-performance liquid chromatography (HPLC) analysis was conducted on an Agilent 1200 (Marshall Scientific, USA). US irradiation for sonodynamic therapy was conducted by hand-held ultrasonic treatment (NSE-UPH-I, Nasonic Co., China).

High-Performance Liquid Chromatography (HPLC) Analysis: HPLC analysis was conducted on an Agilent 1200 (Marshall Scientific, USA). The separation for TPEN was performed using a Zorbax SB-C18 5 µm column (250 mm x 4.6 mm) under the following gradient. Solvent A: ACN. Solvent B: 0.05% TFA. The gradient was mixed from solvents A and B: 0–8 min, 10% A–90% A; 8–13 min, 90% A; 13–13.1 min, 90% A–10% A; 13.1–16 min, 10% A. The volume injected was 2.0 µL at a flow rate of 1.0 mL min^{-1}. TPEN was monitored using a UV detector at 214 nm.

In Vitro Drug Release: 3 mL of fresh PBS was placed in a dialysis tube (MWCO: 1 kDa; Spectra/Por, USA). The dialysis tube was then immersed in STCNs PBS solutions (3 mg, 10 mL) under stirring at 100 rpm, 37 °C. Next, 3 mL PBS was removed from the dialysis tube and replaced with fresh PBS at designated time intervals (0, 1, 3, 5, 7, 12, 24, 48, 60, and 72 h). For samples with US irradiation, the samples were thoroughly mixed and stirred during the US irradiation (1 MHz, 50% duty cycle, 1.0 W cm^{-2}) for 10 min to ensure the dissipation of US throughout the sample. All experiments were performed in triplicate.

Singlet Oxygen Generation Analysis via DPBF: For DPBF absorbance, DPBF was mixed with ACN (20 µL, 8 mM), added into STCNs/TCNs solutions (1.5 mg mL^{-1}, 3 mL), and irradiated with US (1 MHz, 50% duty cycle, 1.0 W cm^{-2}) at the specified time intervals (0, 5, 10, 20, and 30 min). The absorption spectra were then measured using a UV–vis spectrophotometer. During US irradiation, all samples were mixed and stirred to ensure the dispersion of ultrasonic energy throughout the sample. All experiments were performed in triplicate.

Cell Culture: Human liver cancer cell line HuH-7, mice hepatocellular carcinoma cell line Hep1-6, mice hepatocyte cell line AML-12, human pancreatic ductal adenocarcinoma cell line PANC-1, human gallbladder carcinoma cell lines GBC-SD and NOZ were originally purchased from the Shanghai Institute for Biological Science, Chinese Academy of Science (Shanghai, China). NOZ, Hep1-6, HuH-7, AML-12, and PANC-1 were cultured in Dulbecco's Modified Eagle Medium (DMEM) supplemented with 10% fetal bovine serum (FBS) and 1% penicillin/streptomycin at 37 °C in 5% CO_2. GBC-SD were cultured in Roswell Park Memorial Institute (RPMI) 1640 supplemented with 10% fetal bovine serum (FBS) and 1% penicillin/streptomycin at 37 °C in 5% CO_2.

Cellular Uptake: HuH-7, Hep1-6, and AML-12 cells were exposed to STCNs in DMEM to verify cellular uptake. HuH-7 cells (5×10^4 mL^{-1}), Hep1-6 cells (5×10^4 mL^{-1}), and AML-12 cells (5×10^4 mL^{-1}) were seeded in 500 µL medium in 24-well cell culture plates and incubated overnight, and then STCNs (4.9 µg mL^{-1}) were added to the plates. After incubating for 4, 12, and 24 h, cells were washed with PBS three times. The samples were fixed with 4% paraformaldehyde for 10 min and incubated with DAPI (0.01%) for 10 min. Cellular uptake at different time points was monitored by fluorescent microscopy, EVOS FL Auto 2 (Thermo Fisher Scientific, USA).

Cryo-TEM Cell Imaging: HuH-7 cells (1.5×10^6 mL^{-1}) and Hep1-6 cells (1.5×10^6 mL^{-1}) were seeded in 6 cm Petri dishes until adherent and replaced with STCNs (4.9 µg mL^{-1}). After incubation for 4, 12, and 24 h, the cells were first fixed with 2.5% glutaraldehyde in PBS (0.1 M, pH 7.0) overnight, washed three times with PBS, and post-fixed with 1% OsO_4 in PBS for 1 h and washed three times with PBS. Next, the cell samples were dehydrated by a graded series of ethanol (30%, 50%, 70%, 80%) and acetone (90%, 95%, 100%) for 15 min. The cell samples were then placed in a mixture of 1:1 and 1:3 acetone and Spurr resin mixture for 1 and 3 h, respectively, and transferred to the final Spurr resin mixture overnight. Finally, the specimens were placed in Spurr resin and heated to 70 °C for 9 h and were sectioned into ultrathin slices with LEICA EM UC7. The sections were then stained with uranyl acetate and alkaline lead citrate for 10 min. The morphology was observed using TEM microscopy, Talos L120C (Thermo Fisher Scientific, USA) at 120 kV.

Cell Counting Kit-8 (CCK-8) Assay: The in vitro cytotoxicity of nanoparticles was measured using the CCK-8 (Yeasen, Shanghai) assay according to the manufacturer's instructions. HuH-7, Hep1-6, and AML-12 cells were seeded into 96-well cell culture plates at 0.6×10^4 per well until adherent and replaced with TPEN (31.6 nM-100 µM) or STCNs (31.6 nM-100 µM, TPEN concentration in STCNs) in different concentrations and incubated for 24 h. After an additional 48 h, the absorbance was measured by a microplate reader (Thermo Fisher Scientific, USA) at 450 nm. All experiments were performed in triplicate.

Cell damage caused by ROS production from SCNs in nanoparticles under US irradiation was measured in the same manner. HuH-7 and Hep1-6 cells were seeded into 96-well cell culture plates at 0.6×10^4 per well until adherent and replaced with SCNs (0.14–453 µg mL^{-1}) in different concentrations for 24 h incubation. After the removal of nanoparticles, cells were transferred into fresh media and treated with US irradiation (1 MHz, 50% duty cycle, 1.0 W·cm^{-2}) for 5 min. The cells were then incubated at 37 °C for an additional 48 h before measuring on a microplate reader at 450 nm to determine their viability relative to the control unirradiated cells. All experiments were performed in triplicate.

Likewise, the effect of nanoparticles on HCC cell proliferation was also measured by CCK-8 assay. HuH-7 and Hep1-6 cells were seeded in 96-well plates at 0.6×10^4 per well until adherent and replaced with different media for 24 h incubation. Briefly, each cell line was divided into 8 groups: 1) NC (normal media), 2) NC (normal media) with US irradiation, 3) TPEN (1 µM for HuH-7 cells; 0.1 µM for Hep1-6 cells respectively), 4) TPEN (1 µM for HuH-7cells; 0.1 µM for Hep1-6 cells respectively) with US irradiation, 5) SCNs (the same nanoparticle concentration as group 7), 6) SCNs (the same nanoparticle concentration as group 7) with US irradiation, 7) STCNs (1 µM, TPEN concentration in STCNs for HuH-7 cells; 0.1 µM, TPEN concentration in STCNs for Hep1-6 cells respectively), and 8) STCNs (1 µM, TPEN concentration in STCNs for HuH-7 cells; 0.1 µM, TPEN concentration in STCNs for Hep1-6 cells respectively) with US irradiation. After the removal of old media, cells were transferred into fresh media, and groups 2, 4, 6, and 8 were treated with US irradiation (1 MHz, 50% duty cycle, 1.0 W·cm^{-2}) for 5 min. The cells were then incubated at 37 °C for an additional 48 h before measuring on a microplate reader at 450 nm to determine their viability relative to the control unirradiated cells. All experiments were performed in triplicate.

Furthermore, the effect of nanoparticles on other cancer cell proliferation was verified in the same methods mentioned previously. Each cancer cell line was divided into 8 groups: 1) NC (normal media), 2) NC (normal media) with US irradiation, 3) TPEN (1 µM), 4) TPEN (1 µM) with US irradiation, 5) SCNs (the same nanoparticle concentration as group 7), 6) SCNs (the same nanoparticle concentration as group 7) with US irradiation, 7) STCNs (1 µM, TPEN concentration in STCNs), and 8) STCNs (1 µM, TPEN concentration in STCNs) with US irradiation.

Western Blotting: For validation of the cuproptosis mechanism, HuH-7 and Hep1-6 cells were seeded in 6-well plates at a density of 4×10^5 per well until adherent and replaced with different media. Each cell line was also divided into 8 groups and treated as in the cell proliferation assay mentioned previously. After 48 h, the protein was extracted from each cell

group. Then, western blotting was performed according to the standard methods. The following antibodies, Anti-ADX (ab108257), Anti-Pyruvate Dehydrogenase E2 (ab172617), Anti-Lipoic Acid (ab58724), and anti-beta actin (ab8226) were obtained from Abcam.

ROS Assays: HuH-7 and Hep1-6 cells were seeded in 24-well plates at 1×10^5 per well until adherent and replaced with different media for 24 h incubation. Each cell line was also divided into 8 groups and treated as mentioned previously. 4 h after US irradiation, for flow cytometry analysis, adherent cells of all groups were harvested and washed with PBS 3 times; for observation of the fluorescence cell imager, adherent cells of all groups were washed with PBS 3 times. Next, each group was stained with 500 µL (25 µM) 2,7-dichlorodihydrofluorescein diacetate (Sigma–Aldrich, USA) for 30 min at 37 °C in the dark and washed with PBS 3 times. The cells were then immediately analyzed by flow cytometry (BD LSRFortessa, USA) and observed by a fluorescence cell imager (Bio-Rad, USA), respectively. All experiments were performed in triplicate.

SOD and GSH Assays: HuH-7 and Hep1-6 cells were seeded in 6-well plates at a density of 4×10^5 per well until adherent and replaced with different media for 24 h incubation. Each cell line was also divided into 8 groups and treated as mentioned previously. 4 h after US irradiation, adherent cells of all groups were harvested and washed with PBS 3 times, then intracellular SOD and GSH levels were analyzed using the total SOD activity detection kit (Beyotime, China) and GSH and GSSG test kit (Beyotime, China) according to the manufacturer's instructions, respectively.

Transcriptomic Analysis by RNA-seq: To obtain RNA, all samples were washed with PBS, scraped with a "rubber policeman" in lysis buffer, and subjected to the RNeasy Mini Kit (QIAGEN, Hilden, Germany) following the manufacturer's instructions. Isolated total RNA was reverse transcribed to cDNA using a commercial kit (Promega Corporation, Madison, WI, USA) following the manufacturer's instructions. The reaction mixture was heated at 42 °C for 30 min followed by enzyme inactivation at 90 °C for 2 min. The RNA samples were sequenced by Arraystar (Rockville, MD, USA), and cDNAs were used for real-time quantitative reverse transcription PCR (qRT-PCR).

In Vitro ICD Induction Evaluation: To detect the activation of ICD by STCNs, calreticulin (CRT) expression, high mobility group box 1 (HMGB1) expression, and ATP secretion was measured. HuH-7 and Hep1-6 cells were cultured in confocal dishes, divided into 8 groups, and treated as mentioned previously. 4 h after US irradiation, the cells were stained with anti-CRT (Proteinetch, 27298-1-AP) or anti-HMGB1 (Proteinetch, 10829-1-AP) primary antibody and dylight 488 secondary antibody (Boster, BA1127) or dylight 647 secondary antibody (Boster, BA1150) and finally visualized by CLMS. ATP secretion was measured using an ATP detection kit (Beyotime, China) according to the manufacturer's instructions.

In Vitro DC Maturation: Bone-marrow-derived DCs (BMDCs) were extracted and used to study the effect of STCNs on DC maturation in vitro. Immature BMDCs were incubated with HuH-7 and Hep1-6 cells that were divided into 8 groups and treated like the cell proliferation assay mentioned previously for 12 h, respectively. Then, $CD80^+$ $CD86^+$ DCs (mature DCs) in the $CD11c^+$DCs were detected by flow cytometry.

Subcutaneous Tumor Model: C57BL/6J mice (4 weeks old) were obtained from Shanghai SLAC Laboratory Animal Co., Ltd. All animals were bred in a pathogen-free facility with a 12 h light/dark cycle at 20 ± 3 °C and 40–50% humidity and had ad libitum access to food and water. Hep1-6 cells (2×10^6 cells) in 100 µL PBS were subcutaneously injected into the right armpit of each C57BL/6J mouse. The mouse was euthanized when its tumor exceeded the pre-specified maximal tumor volume of 1 cm^3 or when its maximum weight loss exceeded 20%, as required by animal ethics. All animal procedures were performed following the Guidelines for Care and Use of Laboratory Animals of Zhejiang University (Protocol No. 24594).

Fluorescence Imaging In Vivo and Ex Vivo: For fluorescence imaging, tumor-bearing model mice received separate intravenous injections of free TCPP, STNs, and STCNs (10 days after Hep1-6 implant). Fluorescence images (λex = 430 nm; λem = 650 nm) of the mice were acquired by the NIR imaging system (PerkinElmer IVIS Lumina LT, USA) at pre-injection and 1, 4, 8, 12, 24, and 36 h post-injection. Similarly, STCNs were administered by intravenous injection separately for tumor-bearing model mice. Next, the mice were sacrificed at different time points (pre, 1, 4, 8, 12, 24, 36 h) after intravenous injection, with the heart, liver, spleen, lung, kidney, and tumor excised for the observation of the biodistribution of nanoparticles via imaging.

Tumor Inhibition Experiment: For treatment, model mice were randomly divided into 8 groups (n = 8, 5 for monitoring survival and 3 for histological analysis): 1) PBS, 2) PBS with US irradiation, 3) TPEN (1.5 mg kg^{-1}, equivalent to the dose loaded in STCNs), 4) TPEN (1.5 mg kg^{-1}, equivalent to the dose loaded in STCNs) with US irradiation, 5) SCNs (16 mg kg^{-1}), 6) SCNs (16 mg kg^{-1}) with US irradiation, 7) STCNs (17.5 mg kg^{-1}), and 8) STCNs (17.5 mg kg^{-1}) with US irradiation. The dosage of TPEN was within the range of clinically attainable levels. The mice were intravenously injected with 200 µL of the respective formulations three times a week for a total of 9 times. Groups 2, 4, 6, and 8 were irradiated by US (1 MHz, 50% duty cycle, 1.0 W·cm^{-2}) for 15 min at 8 h post-injection. The tumor volume of the mice changed and the mice's body weight was monitored every 3 days. After 26 days of treatment, the mice were euthanized and the tumor tissue was collected, fixed in 4% paraformaldehyde, and embedded in paraffin. Paraffin-embedded tissue slices then underwent H&E, Ki-67-antigen. Meanwhile, all the mice were observed for survival assessment.

Immunofluorescence: To detect the activation of ICD and infiltration of cytotoxic T cells by STCNs in vivo, $CD45^+$ and $CD8a^+$ expression in tumor tissues was measured from Hep1-6 bearing mice that were divided into 8 groups and treated as in the tumor inhibition experiment mentioned previously. The tissue sections were stained with anti-CD45 (Proteinetch, 80297-1-RR) and anti-CD8a (Biolegend, 100724) primary antibody and corresponding secondary antibody, and finally visualized by CLMS.

Bio-Safety Assessment: Normal C57BL/6J mice at the age of 5–6 weeks were randomly divided into two groups (n = 3). Healthy mice were intravenously injected three times a week for a total of 9 times with 200 µL of STCNs solution (17.5 mg kg^{-1}, irradiated by ultrasound for 15 min at 8 h post-injection, 1 MHz, 50% duty cycle, 1.0 W·cm^{-2}), and healthy mice with PBS injection were used as the control group. For histopathological analyses of major organs, different groups of mice were sacrificed on day 30 of treatment to collect the major organs (heart, liver, spleen, lung, and kidney). The tissue samples were fixed in a 4% paraformaldehyde solution, stained with hematoxylin and eosin, and examined under a digital microscope. For blood analysis, complete blood investigation and serum biochemistry assays were carried out by collecting 600 µL of blood from the mice. The white blood cells (WBC), red blood cells (RBC), platelets (PLT), mean corpuscular volume (MCV), mean corpuscular hemoglobin (MCH), and hemoglobin concentration (MCHC) were measured. Blood biochemical examination parameters, including alanine aminotransferase (ALT), aspartate aminotransferase (AST), albumin (ALB), direct bilirubin (DBIL), creatinine (CR), total cholesterol (T-C), and triglyceride (TG).

Evaluation of Pharmacokinetics In Vivo: A 100 µL suspension of STCNs (17.5 mg kg^{-1}) was administered intravenously to C57BL/6J mice through tail vein injection. Subsequently, blood samples were collected retroorbitally from the left eye at 15 min, 30 min, 1 h, 4 h, 8 h, 12 h, 24 h, and 36 h post-administration. The collected blood samples were analyzed using the Tecan Spark multimode microplate reader. To account for any variability in the injection process, the fluorescence intensity of each sample was normalized to that of the initial 15 min time point.

Evaluation of Immunological Effect in Living Mice: On day 10 after different treatments, tumors were extracted from mice to measure the contents of T cells, and tumor-draining lymph nodes were extracted for analysis of dendritic cells (DCs). The experiment procedures were briefly described as follows: the isolated tissues were homogenized and filtered with 70 µm cell filters, and T cells were isolated with lymphocyte separation solution after centrifugation. The collected DCs and T cells were stained with antibodies at 4 °C and then analyzed by flow cytometer. The primary tumors were also collected from different treated mice and used for multicolor immunofluorescence staining of CD8, Foxp3, and Gr1.

Evaluation of Primary Tumor Suppression with Anti-PD-1: To assess the suppression of primary tumors, C57BL/6 mice (5–6 weeks) were used to establish a primary tumor model by implanting Hep1-6 cells in the right flank as mentioned above. Tumor-bearing mice were randomly divided into 3 groups as soon as the tumor grew to 50 mm^3 (n = 5): 1) PBS, 2)

PBS + anti-PD-1 (200 μg PD-1 antibody) group, 3) STCNs (17.5 mg kg^{-1}) + anti-PD-1 (200 μg PD-1 antibody) group. Each group was irradiated by US (1 MHz, 50% duty cycle, 1.0 W·cm^{-2}) for 15 min at 8 h post-injection. In total, four treatments were administered, with tumor size and body weight monitored every 2–3 days.

Statistical Analysis: Statistical analyses were performed using OriginPro 9.5.1 and GraphPad Prism 9. Data are expressed as the means ± SD. The student's *t*-test was used to compare the differences between the two groups. Differences between the means of multiple groups were compared by one-way analysis of variance (ANOVA), followed by Tukey's multiple comparison test. $p < 0.05$ was considered statistically significant. All *p*-values were two-tailed.

Supporting Information

Supporting Information is available from the Wiley Online Library or from the author.

Acknowledgements

T.X., Y.S., W.T., and T.Y. contributed equally to this work. This work was supported by the National Natural Science Foundation of China (No. 82473007, W2433188), Zhejiang Provincial Natural Science Foundation of China (No. LR25H160001), State Key Laboratory of Advanced Drug Delivery and Release Systems (DSQZ-QN-202303) and the Youth Development Fund Program of Sir Run Run Shaw Hospital, Zhejiang University School of Medicine (No. YQNPY20240204041). The authors would like to thank Chaogang Xing and Lijuan Mao from the Analysis Center of Agrobiology and Environmental Sciences, Zhejiang University; Yu Liu and Xinhang Jiang from the College of Life Sciences, Zhejiang University; Li Xu and Qun Pu from the State Key Laboratory of Chemical Engineering, Zhejiang University; Zijing Wang from the State Key Laboratory of Silicon and Advanced Semiconductor Materials, Zhejiang University; and Guoqing Zhu from the Center for Electron Microscopy of Zhejiang University for their technical assistance in nanoparticle characterization; as well as Yuchen Zhang from the Center of Cryo-Electron Microscopy (CCEM), Zhejiang University for technical assistance on Cryo-TEM. The figures in this article were created using Adobe Illustrator, Adobe Photoshop, BioRender, and Microsoft PowerPoint.

Conflict of Interest

The authors declare that there are no conflicts of interest.

Data Availability Statement

All data generated or analyzed during this study are included in this published article (and its Supplementary Information files). All other data are available from the corresponding authors upon request.

Keywords

cuproptosis, hepatocellular carcinoma, immunogenic cell death, metal-organic frameworks, sonodynamic therapy

Received: March 4, 2025
Revised: July 2, 2025
Published online: July 21, 2025

[1] J. M. Llovet, R. Pinyol, R. K. Kelley, A. El-Khoueiry, H. L. Reeves, X. W. Wang, G. J. Gores, A. Villanueva, *Nat. Cancer* **2022**, *3*, 386.
[2] X. Luo, X. He, X. Zhang, X. Zhao, Y. Zhang, Y. Shi, S. Hua, *MedComm* **2024**, *5*, 474.
[3] J. Chen, J. Han, T. Yang, M. Su, S. Cai, *Endoscop. Robot. Surg.* **2023**, *6*, 160.
[4] Q. Zeng, J. Wang, *Endoscop. Robot. Surg.* **2023**, *6*, 16.
[5] J. M. Llovet, F. Castet, M. Heikenwalder, M. K. Maini, V. Mazzaferro, D. J. Pinato, E. Pikarsky, A. X. Zhu, R. S. Finn, *Nat. Rev. Clin. Oncol.* **2021**, *19*, 151.
[6] J. M. Llovet, R. Pinyol, M. Yarchoan, A. G. Singal, T. U. Marron, M. Schwartz, E. Pikarsky, M. Kudo, R. S. Finn, *Nat. Rev. Clin. Oncol.* **2024**, *21*, 294.
[7] D. J. Zabransky, M. Yarchoan, E. M. Jaffee, *Annu. Rev. Cancer Biol.* **2023**, *7*, 149.
[8] G. R. Khosravi, S. Mostafavi, S. Bastan, N. Ebrahimi, R. S. Gharibvand, N. Eskandari, *Cancer Commun.* **2024**, *44*, 521.
[9] P. Tsvetkov, S. Coy, B. Petrova, M. Dreishpoon, A. Verma, M. Abdusamad, J. Rossen, L. Joesch-Cohen, R. Humeidi, R. D. Spangler, J. K. Eaton, E. Frenkel, M. Kocak, S. M. Corsello, S. Lutsenko, N. Kanarek, S. Santagata, T. R. Golub, *Science* **2022**, *375*, 1254.
[10] H. Wu, Z. Zhang, Y. Cao, Y. Hu, Y. Li, L. Zhang, X. Cao, H. Wen, Y. Zhang, H. Lv, X. Jin, *Adv. Sci.* **2024**, *11*, 2401047.
[11] W. Tang, J. Wu, L. Wang, K. Wei, Z. Pei, F. Gong, L. Chen, Z. Han, Y. Yang, Y. Dai, X. Cui, L. Cheng, *ACS Nano* **2024**, *18*, 10495.
[12] B. Geng, J. Hu, X. He, Z. Zhang, J. Cai, D. Pan, L. Shen, *Adv. Mater.* **2024**, *36*, 2313670.
[13] S. Sen, M. Won, M. S. Levine, Y. Noh, A. C. Sedgwick, J. S. Kim, J. L. Sessler, J. F. Arambula, *Chem. Soc. Rev.* **2022**, *51*, 1212.
[14] L. Zhang, N. Montesdeoca, J. Karges, H. Xiao, *Angew. Chem., Int. Ed.* **2023**, *62*, 202300662.
[15] M. Ding, Y. Zhang, N. Yu, J. Zhou, L. Zhu, X. Wang, J. Li, *Adv. Mater.* **2023**, *35*, 2302508.
[16] D. Tang, G. Kroemer, R. Kang, *Nat. Rev. Clin. Oncol.* **2024**, *21*, 370.
[17] Y. Guo, Y. Xu, Q. Bao, C. Shen, D. Ni, P. Hu, J. Shi, *ACS Nano* **2021**, *15*, 16286.
[18] T. C. Wang, N. A. Vermeulen, I. S. Kim, A. B. F. Martinson, J. F. Stoddart, J. T. Hupp, O. K. Farha, *Nat. Protoc.* **2015**, *11*, 149.
[19] X. Zhao, Z. Zhang, X. Cai, B. Ding, C. Sun, G. Liu, C. Hu, S. Shao, M. Pang, *ACS Appl. Mater. Interfaces* **2019**, *11*, 7884.
[20] X. Zhao, S. Liu, C. Hu, Y. Liu, M. Pang, J. Lin, *ACS Appl. Bio Mater.* **2019**, *2*, 4436.
[21] S. Juengpanich, S. Li, T. Yang, T. Xie, J. Chen, Y. Shan, J. Lee, Z. Lu, T. Chen, B. Zhang, J. Cao, J. Hu, J. Yu, Y. Wang, W. Topatana, Z. Gu, X. Cai, M. Chen, *Nat. Commun.* **2023**, *14*, 5699.
[22] S. Li, S. Juengpanich, W. Topatana, T. Xie, L. Hou, Y. Zhu, J. Chen, Y. Shan, Y. Han, Z. Lu, T. Chen, C. Topatana, B. Zhang, J. Cao, J. Hu, J. Yan, Y. Chen, Z. Gu, J. Yu, X. Cai, M. Chen, *Sci. Bull.* **2024**, *69*, 1286.
[23] M. Liu, J. Tu, Y. Feng, J. Zhang, J. Wu, *J. Nanobiotechnol.* **2020**, *18*, 114.
[24] J. Y. Choi, T. Ramasamy, S. Y. Kim, J. Kim, S. K. Ku, Y. S. Youn, J.-R. Kim, J.-H. Jeong, H.-G. Choi, C. S. Yong, J. O. Kim, *Acta Biomater.* **2016**, *39*, 94.
[25] G. Kroemer, C. Galassi, L. Zitvogel, L. Galluzzi, *Nat. Immunol.* **2022**, *23*, 487.
[26] S. Lu, Y. Li, Y. Yu, *Adv. Mater.* **2024**, *36*, 2404971.
[27] F. Hu, J. Huang, T. Bing, W. Mou, D. Li, H. Zhang, Y. Chen, Q. Jin, Y. Yu, Z. Yang, *Adv. Sci.* **2024**, *11*, 2309388.
[28] B. Geng, J. Hu, Y. Li, S. Feng, D. Pan, L. Feng, L. Shen, *Nat. Commun.* **2022**, *13*, 5735.
[29] C. Liu, L. Guo, Y. Wang, J. Zhang, C. Fu, *Coord. Chem. Rev.* **2023**, *494*, 215332.
[30] K. Hadian, B. R. Stockwell, *Nat. Rev. Drug Discovery* **2023**, *22*, 723.
[31] P. Zheng, C. Zhou, L. Lu, B. Liu, Y. Ding, *Journal of Experimental & Clinical Cancer Research* **2022**, *41*, 271.
[32] W.-H. Chen, Q.-W. Chen, Q. Chen, C. Cui, S. Duan, Y. Kang, Y. Liu, Y. Liu, W. Muhammad, S. Shao, C. Tang, J. Wang, L. Wang, M.-H. Xiong,

L. Yin, K. Zhang, Z. Zhang, X. Zhen, J. Feng, C. Gao, Z. Gu, C. He, J. Ji, X. Jiang, W. Liu, Z. Liu, H. Peng, Y. Shen, L. Shi, X. Sun, et al., *Sci. China: Chem.* **2022**, *65*, 1010.
[33] J. Wu, L. Wang, W. Tang, X. Cui, K. Wei, S. Cheng, Z. Pei, H. Lei, Z. Liu, L. Cheng, *Mater. Today* **2023**, *68*, 164.
[34] T. C. Pham, V.-N. Nguyen, Y. Choi, S. Lee, J. Yoon, *Chem. Rev.* **2021**, *121*, 13454.
[35] Y. Cao, S. Liu, Y. Ma, L. Ma, M. Zu, J. Sun, F. Dai, L. Duan, B. Xiao, *Small* **2022**, *18*, 2203466.
[36] Y. Zhang, X. Zhang, H. Yang, L. Yu, Y. Xu, A. Sharma, P. Yin, X. Li, J. S. Kim, Y. Sun, *Chem. Soc. Rev.* **2021**, *50*, 11227.
[37] S. Son, J. H. Kim, X. Wang, C. Zhang, S. A. Yoon, J. Shin, A. Sharma, M. H. Lee, L. Cheng, J. Wu, J. S. Kim, *Chem. Soc. Rev.* **2020**, *49*, 3244.
[38] X. Lin, J. Song, X. Chen, H. Yang, *Angew. Chem., Int. Ed.* **2020**, *59*, 14212.
[39] M. Yuan, S. Liang, Y. Zhou, X. Xiao, B. Liu, C. Yang, P. a. Ma, Z. Cheng, J. Lin, *Nano Lett.* **2021**, *21*, 6042.
[40] E. J. Ge, A. I. Bush, A. Casini, P. A. Cobine, J. R. Cross, G. M. DeNicola, Q. P. Dou, K. J. Franz, V. M. Gohil, S. Gupta, S. G. Kaler, S. Lutsenko, V. Mittal, M. J. Petris, R. Polishchuk, M. Ralle, M. L. Schilsky, N. K. Tonks, L. T. Vahdat, L. Van Aelst, D. Xi, P. Yuan, D. C. Brady, C. J. Chang, *Nat. Rev. Cancer* **2021**, *22*, 102.
[41] L. Chen, J. Min, F. Wang, *Signal Transduct. Target. Ther.* **2022**, *7*, 378.
[42] D. Zhang, S. Tian, Y. Liu, M. Zheng, X. Yang, Y. Zou, B. Shi, L. Luo, *Nat. Commun.* **2022**, *13*, 6835.
[43] J.-T. Li, H. Yang, M.-Z. Lei, W.-P. Zhu, Y. Su, K.-Y. Li, W.-Y. Zhu, J. Wang, L. Zhang, J. Qu, L. Lv, H.-J. Lu, Z.-J. Chen, L. Wang, M. Yin, Q.-Y. Lei, *Signal Transduct. Target. Ther.* **2022**, *7*.
[44] D. Ling, H. Xia, W. Park, M. J. Hackett, C. Song, K. Na, K. M. Hui, T. Hyeon, *ACS Nano* **2014**, *8*, 8027.
[45] S. Liang, X. Deng, P. a. Ma, Z. Cheng, J. Lin, *Adv. Mater.* **2020**, *32*.
[46] J. Xia, Y. Xue, B. Lei, L. Xu, M. Sun, N. Li, H. Zhao, M. Wang, M. Luo, C. Zhang, B. Huang, Y. Du, C.-H. Yan, *Natl. Sci. Rev.* **2021**, *8*.
[47] D. Zhang, Z. Ye, L. Wei, H. Luo, L. Xiao, *ACS Appl. Mater. Interfaces* **2019**, *11*, 39594.